




Unusual layer-by-layer growth of epitaxial oxide islands during Cu oxidation

Meng Li ¹, Matthew T. Curnan ^{1,2}, Michael A. Gresh-Sill¹, Stephen D. House^{1,3}, Wissam A. Saidi ²✉ & Judith C. Yang^{1,3,4}✉

Elucidating metal oxide growth mechanisms is essential for precisely designing and fabricating nanostructured oxides with broad applications in energy and electronics. However, current epitaxial oxide growth methods are based on macroscopic empirical knowledge, lacking fundamental guidance at the nanoscale. Using correlated in situ environmental transmission electron microscopy, statistically-validated quantitative analysis, and density functional theory calculations, we show epitaxial Cu₂O nano-island growth on Cu is layer-by-layer along Cu₂O(110) planes, regardless of substrate orientation, contradicting classical models that predict multi-layer growth parallel to substrate surfaces. Growth kinetics show cubic relationships with time, indicating individual oxide monolayers follow Frank-van der Merwe growth whereas oxide islands follow Stranski-Krastanov growth. Cu sources for island growth transition from step edges to bulk substrates during oxidation, contrasting with classical corrosion theories which assume subsurface sources predominate. Our results resolve alternative epitaxial island growth mechanisms, improving the understanding of oxidation dynamics critical for advanced manufacturing at the nanoscale.

¹Department of Chemical and Petroleum Engineering, University of Pittsburgh, Pittsburgh, PA, USA. ²Department of Mechanical Engineering & Materials Science, University of Pittsburgh, Pittsburgh, PA, USA. ³Environmental TEM Catalysis Consortium (ECC), University of Pittsburgh, Pittsburgh, PA, USA. ⁴Department of Physics and Astronomy, University of Pittsburgh, Pittsburgh, PA, USA. ✉email: alsaidi@pitt.edu; judyang@pitt.edu

Advanced manufacturing of nanostructured metal oxides (MOs) is essential for myriad applications including energy, electronics, sensors, photocatalysts, bio-medicine, and recently for quantum computing^{1–12}. Thus, precise, scalable synthesis and processing of nanostructured MOs are in much demand¹³. Microfabrication methods, such as thermal oxidation, reactive sputtering, and atomic layer deposition, are promising approaches for preparing large batches of epitaxially nanostructured MO^{14,15}. However, current nano-oxide fabrication methods, for which oxidation is a vital step, are empirically based. To better predict and control the shape of nanostructured MOs, a fundamental understanding of the oxide nanocrystal growth process is essential. Established oxidation theories of Wagner¹⁶ and Cabrera–Mott¹⁷ treat the oxidation process exclusively from a macroscopic viewpoint assuming simplified, continuous uniform layers. While these models have been successful in guiding fabrication of amorphous oxide films—such as SiO₂—and corrosion mitigation, they have little predictive power for describing nanostructured MOs due to their lack of atomic crystalline considerations. This shortcoming greatly hinders the industrial manufacturing of nanostructured MOs.

Borrowing from thin-film growth theories, MO nanocrystals that attach to a metal substrate epitaxially during the growth of three-dimensional (3D) oxide islands are explained using the Stranski–Krastanov (layer-plus-island) growth mode^{14,18}. However, this model is defined from an interfacial energy viewpoint, leaving the kinetic process of how these nanostructures form uncertain. One well-accepted kinetic process is the multilayer growth mechanism, which explains the formation of 3D islands as the simultaneous growth of multiple layers stacked parallel to the substrate surface, forming “wedding cake”-shaped islands^{19–21}. For example, islands on (100) substrates form by the concurrent growth of multiple stacked layers along the (100) plane²¹. However, 3D islands with faceted crystal surfaces are also widely observed, such as pyramidal Ge and Si islands in quantum dots^{22–24}, nano-wedge-shaped Fe islands²⁵, and 3D Cu₂O islands on Cu^{26–29}. While these faceted crystal surfaces are at variance with the multilayer growth mechanism, it remains unclear whether the deviations are due to the early or the later stages of the island growth. The lack of direct observation of the growth dynamics at the atomic scale has hindered establishing a fundamental mechanistic explanation for the growth of the 3D epitaxial islands. Recent developments in in situ environmental transmission electron microscopy (ETEM)—with which material systems can be examined under relevant reaction conditions—offer a solution to this problem, enabling the direct observation of growth dynamics^{4,30,31}. However, the results heretofore have been qualitative at best. Extracting statistically meaningful quantitative atomic-scale growth kinetics from the in situ movies, which is critical for understanding atomic-scale growth mechanisms, has become the new challenge.

Herein we perform in situ ETEM oxidation experiments on copper—the most well-studied model material for oxidation that forms epitaxial oxide islands—to provide direct, atomic-scale observations of the growth dynamics of 3D epitaxial oxide islands during oxidation. Quantitative atomic-scale information was extracted using advanced image analysis techniques. By correlating the experimental observations and statistical validation of growth kinetics with density functional theory (DFT) modeling, we present an unusual epitaxial layer-by-layer growth mechanism for the oxide island along a preferred surface facet, unforeseen by previous crystal growth theories.

Results

Layer-by-layer Cu₂O growth along Cu₂O(110). 3D Cu₂O islands were formed by oxidizing single-crystalline Cu films inside the

ETEM at 300 °C under 0.3 Pa O₂. In agreement with previous studies^{32,33}, these Cu₂O islands share cube-on-cube epitaxy with the Cu substrate. The Cu₂O islands on Cu(100) were reported to follow the Stranski–Krastanov (S–K) growth mode, in which a transition from 2D wetting layers to 3D islands was observed beyond a critical thickness³⁴. According to previous models^{33,35}, the oxide is expected to grow along the Cu surface, such as along Cu₂O(100) on Cu(100). However, as shown in Movie S1 and Fig. 1, we found that the Cu₂O islands on both Cu(100) and (110) surfaces (Supplementary Note 1, Supplementary Figs. 2–5, and Supplementary Movies 2–4) grew along the Cu₂O(110) planes in a layer-by-layer adatom growth mode. This is usually observed in Frank–van der Merwe (F–M) growth where the interface mismatch energy is negligible, leading to the formation of a thin-film, instead of islands, along the substrate surface. Our study shows that although the resultant Cu₂O islands follow the S–K growth mode, the formation of each 3D island follows a layer-by-layer growth along a certain plane that is not necessarily parallel to the substrate surface, contradicting classical predictions.

Cu₂O monolayer growth kinetics. To better understand the growth kinetics of each monolayer, we performed quantitative analysis on the boxed area in Fig. 1d on the atomically aligned movie to measure the size evolution of each layer over time (Fig. 1f, Supplementary Note 3). As illustrated in Fig. 1e, each new layer is a 2D flake that grows in both planar directions. Although TEM images only provide 2D through-thickness projections of the growing new layer, given that the two directions are equivalent {110} planes, the projected length evolution in one dimension can be used to estimate the growth in both directions. The nucleation sites of each Cu₂O monolayer (Fig. 1g and Supplementary Fig. S6) were randomly distributed on the previously grown layer, indicating identical nucleation energetic favorability across all sites. Despite that the layer edges typically proceeds in stairs (Fig. 1g), the total projected lengths (*l*) all exhibited a similar smooth growth trend following a cube root relationship with time (*t*): $l^3 = At$ (referred to as cubic relationship for short hereafter, Fig. 1h, Supplementary Fig. 14, and Supplementary Note 3). As a result, the growth rate of the island size is quasi-linear along the [110] direction and cubic along [100] and [010] directions. Interestingly, typical oxide thickness curves found in bulk Cu oxidation experiments in this temperature range also follow cubic rates³⁶, which were explained based on classical oxidation theory¹⁷ due to the formation and diffusion of cation vacancies through an oxide layer that fully covers the metal surface. However, this explanation does not apply to our sample, since the metal surface near the oxide island is still exposed. Instead, we argue that the cubic growth rate of each oxide monolayer could be explained using the diffusion-limited 2D growth kinetics of F–M thin-film growth¹⁹. In this growth mode, a full layer forms by coalescence of several single-monolayer-thick 2D flakes, where each flake grows with $l^3 \sim t$ scaling^{37–39}. The main difference with the thin-film F–M growth is that the observed growth of the oxide monolayer in our samples is due to the nucleation of a single “flake”, rather than many flakes as in thin-films. This difference is likely because the effective substrate for the growth of the oxide layer is relatively small compared to typical thin-film substrates. Presumably, as the MO islands grow in size, layer formation through the coalescence of more than one flake would occur. Hence, the observed $l^3 \sim t$ growth kinetics of each monolayer indicates a diffusion-limited process, possibly due to surface diffusion of Cu and O atoms to form adatoms at the Cu₂O monolayer edge.

The growth trajectories also exhibited coordinated increments and oscillations between multiple layers (Fig. 1g–i). To substantiate

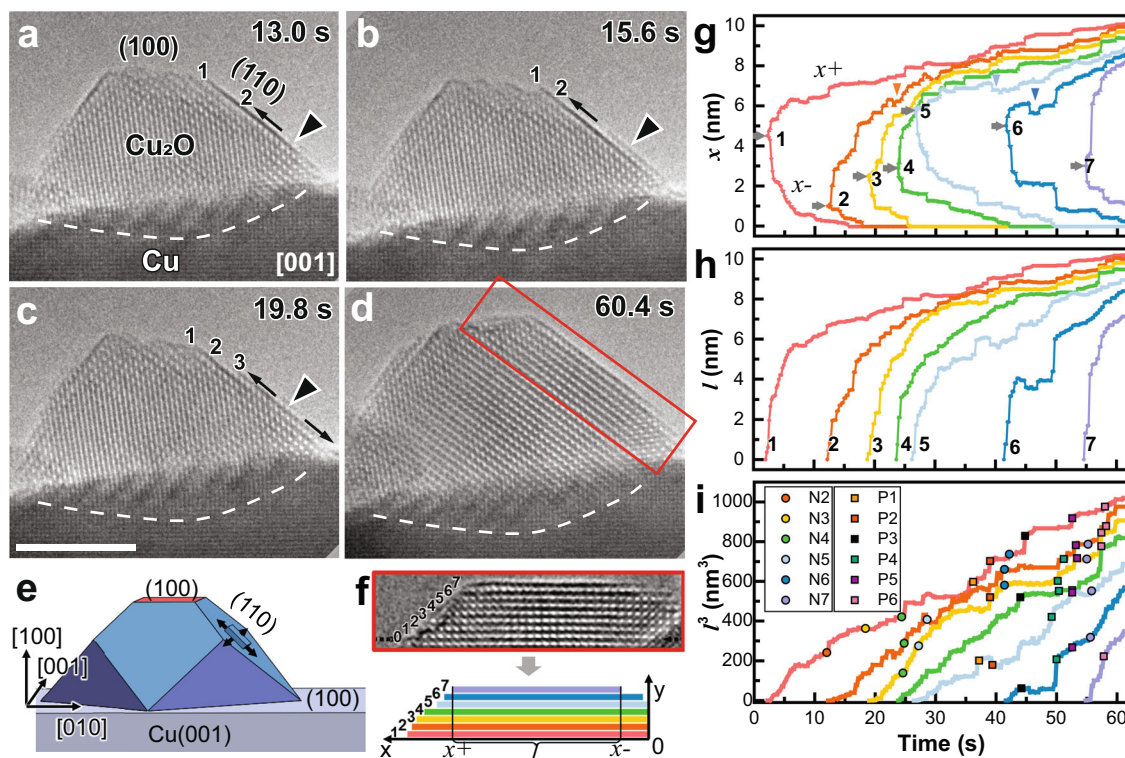


Fig. 1 Layer-by-layer growth of Cu_2O island along $\text{Cu}_2\text{O}(110)$ during $\text{Cu}(100)$ oxidation. **a–c** Snapshots from Supplementary Movie 1 showing adatom growth of the 2nd Cu_2O new layer at 300 °C and $p_{\text{O}_2} = 0.3$ Pa. The layer nucleation site (triangle) and growth direction (arrow) are indicated. Scale bar: 5 nm. **d** The island top forms a flat $\text{Cu}_2\text{O}(100)$ plane over time. **e** Schematic 3D model of the Cu_2O island with a growing new layer. **f** The boxed area from **d**, reoriented for growth trajectory measurement, with a corresponding schematic defining the measured data plotted in **g–i**. **g** Growth trajectory coordinates of the left ($x+$) and right ($x-$) ends of each layer with time, namely when measuring from the right side of the image defined in **f**. Nucleation sites on each layer, marked by gray arrows, indicate a random site distribution. These two ends show stepwise growth with oscillations marked by triangles of matching colors. **h** The projected length (l) of each layer shows a similar trend with smoother curves. **i** Statistically defined breakpoints in growth rates indicate nucleation events (N) and interlayer atom diffusion events (P).

these sudden changes, a multivariate time-series statistical analysis⁴⁰ was performed (l^3 vs. t) to evaluate when breaks in otherwise continuous growth occur^{37,38,41}. The statistically defined structural breaks⁴⁰, shown in Fig. 1i and Supplementary Note 4, are attributed to two types of events, namely the nucleation of new layers (N2–N7) and concerted diffusion events (P1–P6) describing the simultaneous change of growth rates among several layers. Nucleation events generally led to a growth rate decrease in previously grown layers, indicating that Cu and O attachment to the nucleating new layer is preferred over attachment to previous layers. This is likely caused by the Ehrlich–Schwöbel effect, in which downward diffusion across a surface step is prohibited due to an extra energy barrier^{42–44}. Concerted diffusion events generally showed sudden decreases in the growth rates of new layers and increases in those of previous layers. This indicates a cross-layer diffusion of Cu/O sourced from the new Cu_2O monolayer to feed the growth of former layers, which corresponds to adjustment of the top of the Cu_2O island from an initially zig-zagged surface to a flat $\text{Cu}_2\text{O}(100)$ facet (Supplementary Figs. 7–8). Hence, both the oxide monolayer growth trend and variations in monolayer growth indicate a diffusion-limited layer-by-layer growth process resembling the F–M thin-film growth mode, although the overall oxide island follows the S–K mode.

DFT calculations on Cu_2O monolayer growth mechanism. To better understand why the oxide grows along the $\text{Cu}_2\text{O}(110)$ plane in disagreement with classical theories, DFT calculations were

performed to study the earlier-stage atom-by-atom oxide growth events. Gas–solid interfacial energies (γ) were calculated for the (100) and (110) Cu_2O surface planes that are predominantly observed in our experiments. As shown in Fig. 2a and detailed in Supplementary Note 5, Cu_xO_y surface units were sequentially added to these planes to simulate layer growth. For flat Cu_2O surfaces (column *i* in Fig. 2a), Cu–O terminated $\text{Cu}_2\text{O}(110)$ had the lowest γ . Upon adding Cu_xO_y surface units, $\text{Cu}_2\text{O}(110)$ surfaces with exposed Cu–O layers invariably had the lowest γ . These surfaces include structures *i* and *iii* for Cu–O terminated $\text{Cu}_2\text{O}(110)$ and structure *ii* for Cu-terminated $\text{Cu}_2\text{O}(110)$, and their favorability is attributable to their terminal, ionically bonded O–Cu–O chains (Supplementary Figs. 21–23). In contrast, O-terminated $\text{Cu}_2\text{O}(100)$ had the highest γ , regardless of the number of Cu_xO_y surface units added to it. Such instability coincides with the undercoordination of exposed O atoms (Supplementary Fig. 20). Since $\text{Cu}_2\text{O}(100)$ structures must produce less-stable O terminations during its growth, oxide growth along $\text{Cu}_2\text{O}(110)$ is preferable to $\text{Cu}_2\text{O}(100)$. Simulated adatom adsorption events forming Cu_xO_y surface unit *ii* (hollow data points in Fig. 2a and Supplementary Note 6) further support this conclusion. Therefore, γ trend comparisons show that $\text{Cu}_2\text{O}(110)$ forms thermodynamically more favorable flat surfaces, grown Cu_2O monolayers, and single adatom interfaces than $\text{Cu}_2\text{O}(100)$, in agreement with the experimental results.

Nudged elastic band simulations of the diffusion events along the oxide island surface further verified the experimentally observed layer-by-layer growth kinetics along the $\text{Cu}_2\text{O}(110)$ plane (Supplementary Note 7). Figure 2b compares the preferred

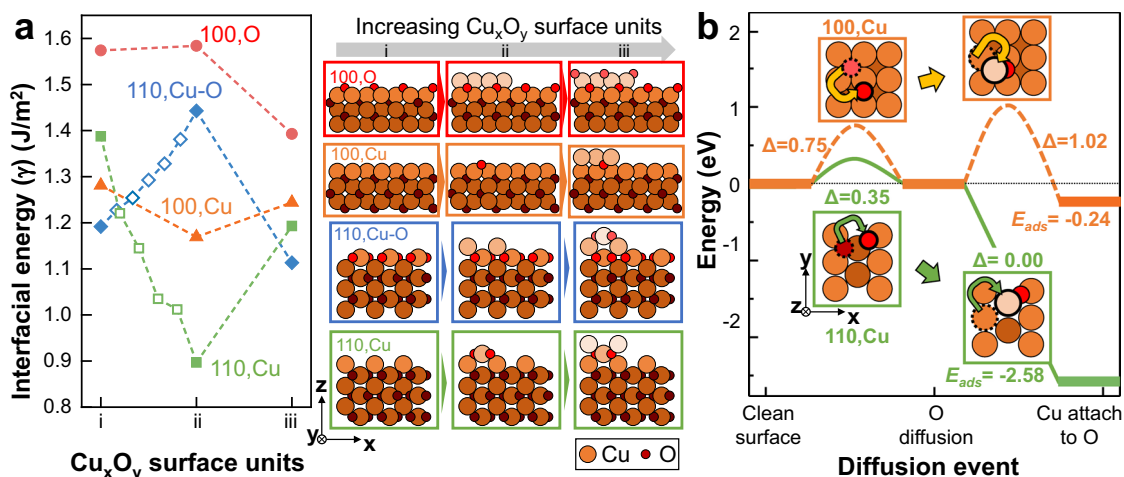


Fig. 2 DFT-calculated interfacial energies and diffusion energies for Cu_2O (110) and (100) surfaces. **a** Most favorable structure γ during Cu_2O monolayer growth for Cu_2O (110) with Cu (green) and Cu–O (blue) terminations, and Cu_2O (100) with Cu (orange) and O (red) terminations. The corresponding atomic structures are shown to the right of the plot, with matching border colors. Hollow data points between *i*–*ii* show adatom adsorption events forming the first Cu_xO_y surface unit. **b** Most-favorable Cu and O diffusion events on Cu_2O surfaces linking diffusion barrier (Δ) and adsorption energy (E_{ads}). Insets with matching border colors show top-down views of the corresponding atomic structures. Cu and O atoms are colored in orange and red, respectively. Brighter/darker colors indicate a higher/lower *z* position.

diffusion mechanisms required to make an oxide layer on Cu terminated Cu_2O (110) and Cu_2O (100) surfaces. The most favorable rate-limiting diffusion process for forming Cu–O layers on Cu-terminated Cu_2O (110) is single O diffusion with inter-channel endpoints (diffusion barrier of $\Delta = 0.35$ eV), and the matching Cu diffusion process to place Cu on top of that O is barrierless with favorable adsorption energy ($E_{\text{ads}} = -2.58$ eV). In comparison, the most favorable rate-limiting O diffusion process on a Cu-terminated Cu_2O (100) surface is in-channel single O diffusion ($\Delta = 0.75$ eV). The matching Cu diffusion process places Cu on top of that O, yielding a large barrier ($\Delta = 1.02$ eV) and less-favorable adsorption energy ($E_{\text{ads}} = -0.24$ eV). The corresponding process for forming Cu layers on Cu–O terminated Cu_2O (110) is in-channel single Cu diffusion ($\Delta = 0.42$ eV, Supplementary Fig. 29). Rate-limiting step comparisons favor Cu_2O (110) over Cu_2O (100) not only across the initial and final states of the oxide layer formation process (0.42 eV vs. 1.02 eV) but also for each transient diffusing atom composition. Therefore, Cu and O prefer to diffuse to Cu_2O (110) island growth fronts over Cu_2O (100) fronts, further validating prior experimental outcomes.

Cu source for Cu_2O island growth. The source of Cu during Cu_2O growth also warranted investigation. Traditional oxidation theory¹⁷ argues that Cu is supplied from the metal||oxide interface through diffusion across the oxide, leading to an interface shift toward the metal side. However, as seen in Figs. 1 and Supplementary Fig. 6, the Cu|| Cu_2O interfaces predominantly remained unchanged during the oxidation process, particularly during the initial period of oxidation when there are few nucleated Cu_2O islands. This indicates that there must be other sources for Cu instead of the substrate Cu. A recent study found Cu_2O island growth with gradual height decreases of the surrounding Cu surface steps⁴⁵, inferring that Cu detaching from step edges might be the source. However, direct evidence for this claim has been lacking. Figure 3 and Supplementary Movie 5 show that during oxidation of Cu(100) facets with several one-atomic-layer-high surface steps, these steps retreated when Cu_2O grew, while the Cu|| Cu_2O interface remained unchanged. Due to the

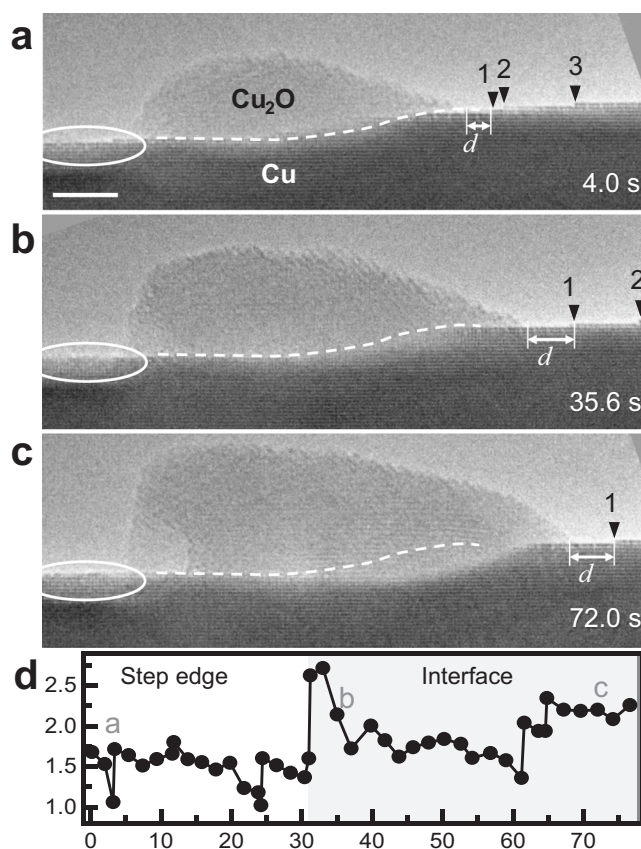


Fig. 3 Cu sources for Cu_2O nano-island growth. **a, b** Cu_2O grows while surface steps (1–3, marked by triangles) retreated and the Cu|| Cu_2O interface (dashed lines) remained unchanged. (Scale bar: 5 nm). **c** When surface steps were far from the Cu_2O island, Cu_2O continued to grow and the Cu|| Cu_2O interface started to migrate towards Cu. **d** A plot of the measured distance (*d*) between the Cu_2O island and step edge “1” with time. *d* suddenly increased at ~31 s, leading to the transition from step edge Cu to bulk Cu consumption.

thickness difference between the Cu film and the Cu₂O island, the amount of Cu lost from the surface steps is comparable to the amount of Cu added to Cu₂O. This indicates that Cu detaching from step edges is the source of Cu for Cu₂O growth in the early oxidation stage. Later, the Cu||Cu₂O interface migrates toward the Cu substrate, indicating that in later stage oxidation, the substrate serves as the Cu source. The transition between Cu sources is determined by the distance from the nearest step edge (Fig. 3d), which is explainable by Cu diffusion. When the oxide island is near a step edge, Cu detached from surface steps can easily diffuse to the oxide island via surface diffusion. However, when there are very few surface steps or the oxide island is far away from the surface steps, bulk Cu diffusion from the Cu substrate to the gas||oxide interface becomes more efficient. As shown in Supplementary Note 8, even on reconstructed Cu surfaces, the diffusion barrier of Cu surface diffusion is still lower than that of bulk diffusion, leading to less-faceted oxide shapes during the interfacial Cu sourcing stage.

Mechanism of 3D Cu₂O island growth. Based on the above discussion and the energetic data summarized in Supplementary Table 7, the mechanism of the unusual epitaxial oxide island growth processes during Cu oxidation, summarized in Fig. 4, is:

- Due to surface reconstruction, O₂ dissociation on the Cu surface is inhibited, so O adatoms are provided by O₂ dissociative adsorption on Cu₂O surfaces^{2,46}. The preferred diffusion barriers and adsorption energies of O on Cu₂O (110) over those on Cu₂O(100) suggest more diffusing O atoms will be present on the Cu₂O(110) surface.
- When there are Cu surface steps nearby, Cu adatoms detached from Cu step edges diffuse to Cu₂O surfaces via surface diffusion. Because of the preferred diffusion barriers and adsorption energies of Cu on Cu₂O(110), more Cu atoms will diffuse on Cu₂O(110) than Cu₂O(100). Due to the lower surface energy of Cu₂O(110) and more favorable adsorption energies of Cu and O on the Cu₂O(110) step, Cu₂O nuclei will form on Cu₂O(110). This is followed by the growth of Cu₂O monolayers in an atomic adsorption process directed toward the growth front of the new layer. The vapor deposition process to grow oxides can be viewed as an extreme case of this scenario, where there are sufficient mobile Cu atoms present to directly react with O atoms⁴⁵.
- The new Cu₂O layer grows in this adatom growth method until the edge of the layer reaches the ridge of the previous Cu₂O layer, then a new Cu₂O layer nucleates following the steps in (a) and (b). This leads to the observed layer-by-layer growth along Cu₂O(110). For each monolayer, the growth of a new Cu₂O layer on the Cu₂O(110) facet follows the diffusion-limited Frank–van der Merwe growth process with cubic growth rate $\beta^3 \sim t$. However, due to the preference of Cu₂O(110) over Cu₂O(100) in both kinetics and energetics, the overall Cu₂O island follows the Stranski–Krastanov growth model. When the Cu surface steps are far away, substrate Cu will feed Cu₂O growth by interfacial diffusion via place exchange with Cu vacancies in Cu₂O islands.

Discussion

Using DFT, we have investigated the energetics of several most probable diffusion paths, and corresponding thermodynamic states, that are proposed to underline studied experimental observations. However, a complete understanding of studied oxide growth dynamics is beyond the capabilities of DFT alone,

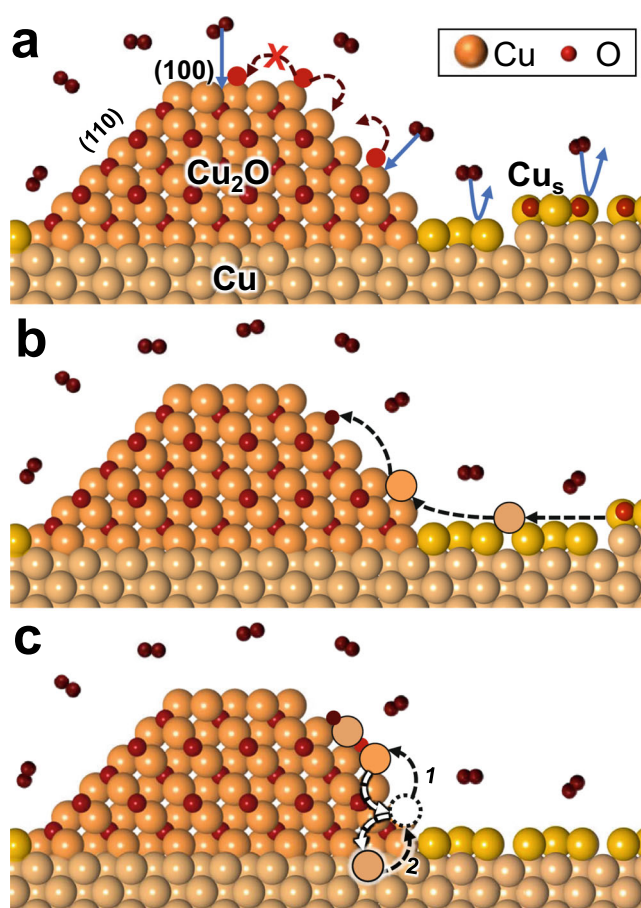


Fig. 4 Schematic of Cu₂O growth mechanism. **a** Dissociative adsorption of O₂ (red atoms) is blocked on the reconstructed Cu surface (Cu_s, gold atoms) and performed on Cu₂O. Given lower diffusion barriers and favorable O adsorption energies on Cu₂O(110), more O atoms segregate toward Cu₂O(110). **b** When Cu steps are nearby, Cu adatoms detached from Cu step edges, diffuse to Cu₂O islands, and attach to O atoms to form Cu₂O monolayers, given favorable Cu and O E_{ads} on Cu₂O(110) steps. **c** When Cu surface steps are far away, substrate Cu will feed the growth of Cu₂O via interface diffusion, namely through place exchange with Cu vacancies (dashed circle). Cu atoms from Cu₂O, the Cu surface, and the Cu bulk are colored orange, gold, and beige, respectively. O atoms are colored dark red.

especially when considering the many possible diffusion processes that induce concerted oxide nucleation and growth processes over multiple island layers. Comparisons between statistical conclusions and ETEM observations made in “Correlating Statistical Results with Experimental Observations” (Supplementary Note 4) demonstrate that limitations in Cu sourced from adjacent island layers contribute to observed island shapes and relative layer growth rates. Therefore, the combination of surface orientations and terminations predicted by simulation, island shape evolution by ETEM observations, and relative growth rates characterized by statistical conclusions, is needed to completely depict oxide growth dynamics.

Our results provide direct, atomic-scale growth dynamics of 3D epitaxial oxide island growth. Instead of multilayer growth along substrate surfaces to form wedding-cake shaped islands, we found the growth of 3D epitaxial oxide islands follows a layer-by-layer growth mechanism along a preferred facet. The growth kinetics of each oxide monolayer is consistent with predictions from the diffusion-limited 2D Frank–van der Merwe growth model for thin-films³⁷. To our knowledge, this is the first atomic-resolution

experimental proof of the atomic-level growth dynamics of 3D islands. Our study sheds new light on the epitaxial oxide growth mechanism and provides a deeper understanding of the dynamic processes involved in initial oxidation, which will ultimately help to precisely predict, design, and control nanostructured oxide growth. Our findings would apply to other metals—such as Al⁴⁷, Ni-Cr^{4,48}, Mo³⁰, Mg^{49,50} and Ag⁵¹—where a similar layer-by-layer oxide growth was observed for the islands, though without confirmation on the early stages. Moreover, this work demonstrates that with meticulous in situ TEM experiments and advanced data analysis, statistically meaningful quantitative atomic-scale growth kinetics can be resolved. When complemented with correlated theoretical simulations, such work will promote the understanding of nanoscale dynamics to a new level.

Methods

Provided in Supplementary Information.

Data availability

All data is available in the main text or the Supplementary Materials (Supplementary Movies S1–S5, Methods, Supplementary Notes 1–8, Supplementary Notes 1–8, Supplementary Figs. 1–31, and Supplementary Tables 1–7).

Code availability

The code for in situ movie analysis and statistical analysis are available from the corresponding author on request.

Received: 3 August 2020; Accepted: 31 March 2021;

Published online: 13 May 2021

References

- Hansen, P. L. Atom-resolved imaging of dynamic shape changes in supported copper nanocrystals. *Science* **295**, 2053–2055 (2002).
- Gattinoni, C. & Michaelides, A. Atomistic details of oxide surfaces and surface oxidation: the example of copper and its oxides. *Surf. Sci. Rep.* **70**, 424–447 (2015).
- Luc W. et al. Two-dimensional copper nanosheets for electrochemical reduction of carbon monoxide to acetate. *Nat. Catal.* **2**, 423–430 (2019).
- Luo, L. et al. Atomic origins of water-vapour-promoted alloy oxidation. *Nat. Mater.* **17**, 1–6 (2018).
- Mortazavi, N. et al. Interplay of water and reactive elements in oxidation of alumina-forming alloys. *Nat. Mater.* **17**, 610–617 (2018).
- Sáenz-Trevizo, A. et al. *Functional Nanostructured Oxides: Synthesis, Properties, and Applications* (Elsevier Inc., 2018).
- McKee, R. A., Walker, F. J. & Chisholm, M. F. Physical structure and inversion charge at a semiconductor interface with a crystalline oxide. *Science* **293**, 468–471 (2001).
- Scully, J. R. The COVID-19 pandemic, part 1: can antimicrobial copper-based alloys help suppress infectious transmission of viruses originating from human contact with high-touch surfaces? *CORROSION* **76**, 523–527 (2020).
- Netzer, F. P. “Small and beautiful” - the novel structures and phases of nano-oxides. *Surf. Sci.* **604**, 485–489 (2010).
- Cong, S., Tian, Y., Li, Q., Zhao, Z. & Geng, F. Single-crystalline tungsten oxide quantum dots for fast pseudocapacitor and electrochromic applications. *Adv. Mater.* **26**, 4260–4267 (2014).
- Chu, Y. H. Van der Waals oxide heteroepitaxy. *npj Quantum Mater.* **2**, 1–5 (2017).
- Zhu, Q., Zou, L., Zhou, G., Saidi, W. A. & Yang, J. C. Early and transient stages of Cu oxidation: atomistic insights from theoretical simulations and in situ experiments. *Surf. Sci.* **652**, 98–113 (2016).
- Basic Energy Sciences(BES) DoE. Basic Research Needs for Transformative Manufacturing (Brochure). (2020).
- Barth, J. V., Costantini, G. & Kern, K. Engineering atomic and molecular nanostructures at surfaces. *Nature* **437**, 671–679 (2005).
- Tersoff, J., Teichert, C. & Lagally, M. G. Self-organization in growth of quantum dot superlattices. *Phys. Rev. Lett.* **76**, 1675–1678 (1996).
- Wagner, C. & Hammen, H. Conductivity and oxygen excess in cuprous oxide. *Z. für. Physikalische Chem.* **40**, 197–206 (1938).
- Cabrera, N. & Mott, N. F. Theory of the oxidation of metals. *Rep. Prog. Phys.* **12**, 308–308 (1949).
- Franchy, R. Growth of thin, crystalline oxide, nitride and oxynitride films on metal and metal alloy surfaces. *Surf. Sci. Rep.* **38**, 195–294 (2000).
- Brune, H. Epitaxial Growth of Thin Films. *Surface and Interface Science*. (eds Wandelt, K.) <https://doi.org/10.1002/9783527680566.ch20> (Wiley-VCH Verlag GmbH & Co. KGaA, 2014).
- Jesson, D. E., Chen, K. M. & Pennycook, S. J. Kinetic pathways to strain relaxation in the Si-Ge system. *MRS Bull.* **21**, 31–37 (1996).
- Michely, T., Krug, J. & Concepts, B. *Layer-By-Layer Growth and Growth Manipulation* (Springer, 2004).
- Medeiros-Ribeiro, G., Bratkovski, A. M., Kamins, T. I., Ohlberg, D. A. A. & Williams, R. S. Shape transition of germanium nanocrystals on a silicon (001) surface from pyramids to domes. *Science* **279**, 353–355 (1998).
- Ross, F. M., Tromp, R. M. & Reuter, M. C. Transition states between pyramids and domes during Ge/Si island growth. *Science* **286**, 1931–1934 (1999).
- Mo, Y. W., Swartzentruber, B. S., Kariotis, R., Webb, M. B. & Lagally, M. G. Growth and equilibrium structures in the epitaxy of Si on Si(001). *Phys. Rev. Lett.* **63**, 2393–2396 (1989).
- Shvets, I. V., Murphy, S. & Kalinin, V. Nanowedge island formation on Mo(1 1 0). *Surf. Sci.* **601**, 3169–3178 (2007).
- Lyubintsev, I., Lea, A. S., Thevuthasan, S. & Baer, D. R. Formation of epitaxial oxide nanodots on oxide substrate: Cu₂O on SrTiO₃(1 0 0). *Surf. Sci.* **589**, 120–128 (2005).
- Markworth, P. R. et al. Coherent island formation of Cu₂O films grown by chemical vapor deposition on MgO(110). *J. Mater. Res.* **16**, 2408–2414 (2001).
- Ottosson, M., Lu, J. & Carlsson, J. O. Chemical vapour deposition of Cu₂O on MgO(100) from CuI and N₂O: aspects of epitaxy. *J. Cryst. Growth* **151**, 305–311 (1995).
- Zhou, G. & Yang, J. C. *In-Situ Electron Microscopy: Applications in Physics, Chemistry and Materials Science*. <https://doi.org/10.1002/9783527652167.ch8> (Wiley-VCH Verlag GmbH & Co. KGaA, 2012).
- Yu J. et al. Atomic mechanism in layer-by-layer growth via surface reconstruction. *Nano Lett.* **19**, 4205–4210 (2019).
- Li, L. et al. Surface-step-induced oscillatory oxide growth. *Phys. Rev. Lett.* **113**, 1–5 (2014).
- Yang, J. C. & Zhou, G. In situ ultra-high vacuum transmission electron microscopy studies of the transient oxidation stage of Cu and Cu alloy thin films. *Micron* **43**, 1195–1210 (2012).
- Zhou, G. & Yang, J. C. Initial oxidation kinetics of Cu(100), (110), and (111) thin films investigated by in situ ultra-high-vacuum transmission electron microscopy. *J. Mater. Res.* **20**, 1684–1694 (2005).
- Zhou, G. et al. In situ atomic-scale visualization of oxide islanding during oxidation of Cu surfaces. *Chem. Commun.* **49**, 10862–10864 (2013).
- Holloway, P. H. & Hudson, J. B. Kinetics of the reaction of oxygen with clean nickel single crystal surfaces. *Surf. Sci.* **43**, 123–140 (1974).
- O'Reilly, M. et al. Investigation of the oxidation behaviour of thin film and bulk copper. *Appl. Surf. Sci.* **91**, 152–156 (1995).
- Bartelt, M. C. & Evans, J. W. Scaling analysis of diffusion-mediated island growth in surface adsorption processes. *Phys. Rev. B* **46**, 12675–12687 (1992).
- Tang, L.-H. Island formation in submonolayer epitaxy. *J. de. Phys. I* **3**, 935–950 (1993).
- Evans, J. W., Thiel, P. A. & Bartelt, M. C. Morphological evolution during epitaxial thin film growth: formation of 2D islands and 3D mounds. *Surf. Sci. Rep.* **61**, 1–128 (2006).
- Chow, G. C. Tests of equality between sets of coefficients in two linear regressions. *Econometrica* **28**, 591–605 (1960).
- Chi, H. et al. In situ environmental TEM observation of two-stage shrinking of Cu 2 O islands on Cu(100) during methanol reduction. *Phys. Chem. Chem. Phys.* **22**, 2738–2742 (2020).
- Zhu, Q., Saidi, W. A. & Yang, J. C. Enhanced mass transfer in the step edge induced oxidation on Cu(100) surface. *J. Phys. Chem. C* **121**, 11251–11260 (2017).
- Zhu, Q., Saidi, W. A. & Yang, J. C. Step-induced oxygen upward diffusion on stepped Cu(100) surface. *J. Phys. Chem. C* **119**, 251–261 (2015).
- Zhu, Q., Saidi, W. A. & Yang, J. C. Step-edge directed metal oxidation. *J. Phys. Chem. Lett.* **7**, 2530–2536 (2016).
- Zhou, G. et al. Step-edge-induced oxide growth during the oxidation of Cu surfaces. *Phys. Rev. Lett.* **109**, 1–5 (2012).
- Yu, X., Zhang, X., Tian, X., Wang, S. & Feng, G. Density functional theory calculations on oxygen adsorption on the Cu₂O surfaces. *Appl. Surf. Sci.* **324**, 53–60 (2015).
- Oh, S. H. et al. Oscillatory mass transport in vapor-liquid-solid growth of sapphire nanowires. *Science* **330**, 489–493 (2010).
- Luo, L. et al. In situ atomic scale visualization of surface kinetics driven dynamics of oxide growth on a Ni-Cr surface. *Chem. Commun.* **52**, 3300–3303 (2016).
- Zheng, H. et al. Direct atomic-scale observation of layer-by-layer oxide growth during magnesium oxidation. *Appl. Phys. Lett.* **104**, 141906–141906 (2014).
- Cao, F. et al. Atomistic observation of structural evolution during magnesium oxide growth. *J. Phys. Chem. C* **120**, 26873–26878 (2016).

51. Zhu, Q. et al. Defect-driven selective metal oxidation at atomic scale. *Nat. Commun.* **12**, 6–13 (2021).

Acknowledgements

We acknowledge Mr. Xianhu Sun (SUNY Binghamton), Drs. Hao Chi and Henry Ayoola (University of Pittsburgh) for helpful discussions and assistance in experiments. The experimental work was performed at the Petersen Institute of NanoScience and Engineering (PINSE) Nanoscale Fabrication and Characterization Facility (NFCF) at University of Pittsburgh. We thank NFCF staff Mr. Matt France and Dr. Susheng Tan for their assistance. This research used resources of the Environmental TEM Catalysis Consortium (ECC), which is supported by the University of Pittsburgh and Hitachi High Technologies. Computational resources were provided by the University of Pittsburgh Center for Research Computing (CRC), the Extreme Science and Engineering Discovery Environment (XSEDE) supported by the National Science Foundation (NSF OCI-1053575), and at the Argonne Leadership Computing Facility, which is a DOE Office of Science User Facility supported under Contract DE-AC02-06CH11357.

Author contributions

J.C.Y. and W.A.S. conceived and directed the project. M.L. conducted the experiments, data analysis, and drafted the manuscript. M.T.C. conducted D.F.T. simulations and statistical analysis. M.A.G. and S.D.H. assisted with the data analysis. All authors contributed to results discussion and manuscript refinement.

Funding

This work is supported by the National Science Foundation (NSF DMR-1410055, NSF DMR-1508417, and NSF CMMI-1905647).

Competing interests

The authors declare no competing interests.

Additional information

Supplementary information The online version contains supplementary material available at <https://doi.org/10.1038/s41467-021-23043-w>.

Correspondence and requests for materials should be addressed to W.A.S. or J.C.Y.

Peer review information *Nature Communications* thanks Nicholas Harrison, Igor Shvets, and the other, anonymous, reviewer(s) for their contribution to the peer review of this work. Peer reviewer reports are available.

Reprints and permission information is available at <http://www.nature.com/reprints>

Publisher's note Springer Nature remains neutral with regard to jurisdictional claims in published maps and institutional affiliations.



Open Access This article is licensed under a Creative Commons Attribution 4.0 International License, which permits use, sharing, adaptation, distribution and reproduction in any medium or format, as long as you give appropriate credit to the original author(s) and the source, provide a link to the Creative Commons license, and indicate if changes were made. The images or other third party material in this article are included in the article's Creative Commons license, unless indicated otherwise in a credit line to the material. If material is not included in the article's Creative Commons license and your intended use is not permitted by statutory regulation or exceeds the permitted use, you will need to obtain permission directly from the copyright holder. To view a copy of this license, visit <http://creativecommons.org/licenses/by/4.0/>.

© The Author(s) 2021